Role of Antiferromagnetic Ordering in the (1×2) Surface Reconstruction of $Ca(Fe_{1-x}Co_x)_2As_2$

Guorong Li,[1] Liangbo Liang,[2] Qing Li,[3] Minghu Pan,[3] V. B. Nascimento,[1] Xiaobo He,[1] A. B. Karki,[1] Vincent Meunier,[2] Rongying Jin,[1] Jiandi Zhang,[1] and E. W. Plummer[1]

[1]*Department of Physics & Astronomy, Louisiana State University, Baton Rouge, Louisiana 70803, USA*

[2]*Department of Physics, Applied Physics, and Astronomy, Rensselaer Polytechnic Institute, Troy, New York 12180, USA*

[3]*Center for Nanophase Materials Sciences, Oak Ridge National Laboratory, Oak Ridge, Tennessee 37831, USA*

(Received 15 July 2013; published 20 February 2014)

Low energy electron diffraction, scanning tunneling microscopy and spectroscopy, and first-principles spin-dependent density functional theory are utilized to investigate the geometric, electronic, and magnetic structures of the stripe-ordered (1×2) surface of $Ca(Fe_{1-x}Co_x)_2As_2$ ($x = 0$, 0.075). The surface is terminated with a 50% Ca layer. Compared to the bulk, the surface Ca layer has a large inward relaxation (~0.5 Å), and the underneath As-Fe_2-As layer displays a significant buckling. First-principles calculations show that the (1×2) phase is stabilized by the bulk antiferromagnetic spin ordering through the spin-charge-lattice coupling. Strikingly, a superconducting gap (~7 meV at 7.4 K) is observed to spatially coexist with the (1×2) phase ($x = 0.075$ compound). This implies the coexistence of both superconductivity and AFM ordering at the surface.

DOI: 10.1103/PhysRevLett.112.077205 PACS numbers: 75.70.Cn, 68.35.B−, 68.37.Ef, 73.20.−r

The discovery of high-temperature superconductivity (SC) in layered Fe-based compounds has brought to the attention of materials community a very interesting class of materials [1–6]. One of the most intriguing aspects of these materials is the coupling of structure, magnetism, and superconductivity. There is a concurrent structural and magnetic transition in AFe_2As_2 (or $A122$ where A = Ba, Sr, Ca) [Fig. 1(a)]: from tetragonal paramagnetic (PM) at high temperatures to orthorhombic antiferromagnetic (AFM) at low temperatures [1,7]. These coupled transitions split and decrease in temperature with chemical doping [Fig. 1(a)] or the application of hydrostatic pressure [8]. Unlike compounds such as $SmFeAsO_{1-x}F_x$ [9] and $CeFeAsO_{1-x}F_x$ [10], superconductivity in $A122$ seems to emerge prior to the complete suppression of AFM [1,7,11]. As shown in Fig. 1(a), $Ca(Fe_{1-x}Co_x)_2As_2$ has an apparent overlap of superconducting and AFM phases in the bulk underdoped region [7]. Unfortunately, at present there is no way to measure the spatially-resolved structure, magnetic order, and superconductivity.

The creation of a surface by cleaving these layered materials disturbs the balance between lattice, charge, and spin, amplifying certain aspects of the coupling seen in the bulk. For the AFe_2As_2 materials, the presence of a surface stabilizes the orthorhombic phase [2,12,13] and presumably, the AFM ordering. For example, the surface of $Ba(Fe_{1-x}Co_x)_2As_2$ exhibits a higher structural transition temperature than observed in the bulk [2], opposite to the effect of hydrostatic pressure to the bulk [8]. It turns out that the surface mimics the bulk properties under uniaxial pressure [14], thus providing a platform to gain insight into the coupling between lattice and magnetic structure under extreme conditions. Topographic measurements of $BaFe_2As_2$ show that the surface structure is stabilized with an enhanced orthorhombicity [12]. The domain structure at $BaFe_2As_2$ surface is further locked by AFM ordering, indicated by the broken mirror symmetry at the domain boundaries [6]. Interestingly, a superconducting energy gap is observed at such a surface [13]. Scanning tunneling studies on $NaFe_{1-x}Co_xAs$ [15] indicate that a spin density wave gap coexists with SC gap. Scanning tunneling microscopy (STM) combined with scanning tunneling spectroscopy (STS) presents a unique capability of correlating structure and electronic properties (including the SC gap) with atomic resolution. What needs to be

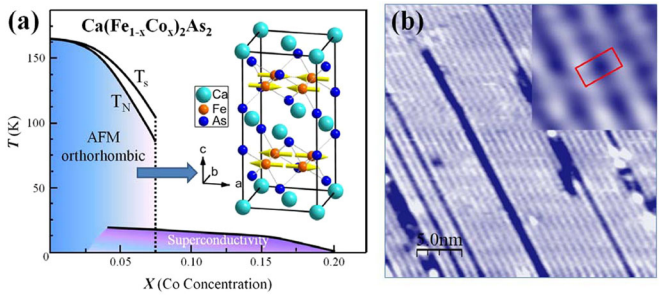

FIG. 1 (color online). (a) Bulk phase diagram of $Ca(Fe_{1-x}Co_x)_2As_2$. Inset is the schematic view of the orthorhombic unit cell with spin structure; (b) STM topography of stripe-ordered surface on $CaFe_2As_2$ at ($V_{bias} = 1.0$ V, $I_t = 200$ pA). Inset is the enlarged image, where the red rectangle shows the (1×2) unit cell.

developed is a way of sensing magnetic order so that STM and STS can be used to map the spin-charge-lattice coupling.

AFM ordering at the surface is difficult to probe directly, and thus has to be determined indirectly. Here, we present a study of the (1×2) surface of $Ca(Fe_{1-x}Co_x)_2As_2$ ($x = 0$, 0.075) by combining low energy electron diffraction (LEED), STM and STS, and density functional theory (DFT) calculations to address the coupling between spin, charge, and lattice. The Ca122 surface was chosen for this study because it is predominantly (1×2) and simpler than its sister compound Ba122 [3]. We first use LEED intensity (I) versus voltage (V) analysis to determine that the (1×2) reconstructed surface is a half monolayer (50%) Ca with a large inward relaxation (~0.5 Å), and with a significant buckling in the underneath As-Fe_2-As layer. Then, first-principles spin-dependent DFT (SDDFT) calculations are performed to demonstrate that the surface lattice structure is reproduced if and only if the surface possesses bulk AFM ordering. A superconducting gap is found at this reconstructed surface by STS, presumably as the consequence of the proximity to superconductivity in the bulk.

Single crystals of $Ca(Fe_{1-x}Co_x)_2As_2$ ($x = 0$, 0.075) were grown out of Sn flux [16]. Magnetic susceptibility and electrical resistivity measurements show the bulk magnetic to structural transition temperature is $T_{N\text{-}S} \sim 170$ K for $x = 0$. For the $x = 0.075$ compound, the bulk $T_N \sim 90$ K and $T_S \sim 100$ K. Superconductivity occurs at $T_c \sim 19$ K (bulk). STM and STS measurements were carried out at 85, 20, 16, and 7.4 K with a home-built variable temperature STM [17] with a tungsten tip at 85 K and Pt/Ir tip at 20, 16, and 7.4 K. For LEED experiments, the sample position was adjusted to achieve normal incidence for the primary electron beam. The LEED patterns were recorded at 85 K over a beam energy range of 40 to 400 eV by a CCD camera with a LabView interface. LEED I-V patterns were collected immediately after the fresh cleave at 85 K.

Plane-wave DFT calculations were performed using the VASP package [18,19] within the generalized gradient approximation using the Perdew-Burke-Enzerhof exchange-correlation functional [20]. Projector augmented wave pseudopotentials [21] were used with a 400 eV energy cutoff. Sampling in the Brillouin zone was $(16 \times 16 \times 8)$ for the bulk and $(8 \times 8 \times 1)$ for the (1×2) surface structure within the Monkhorst-Pack scheme [22]. For the bulk, both atom positions and cell dimensions were relaxed until the residual forces are all lower than 0.02 eV/Å. Then two optimized bulk unit cells [see the inset of Fig. 1(a)] were built along the c-axis direction to model the surface in the repeated slab model with a 14 Å vacuum. The surface was relaxed with in-plane lattice parameters fixed to the bulk ones until all the residual forces were lower than 0.04 eV/Å. For spin-polarized calculations, both the lattice and magnetic moments were determined self consistently to minimize the total energy, starting with a number of different initial spin orderings.

The orthorhombic AFM structure of $Ca(Fe_{1-x}Co_x)_2As_2$ [7] is shown in the inset of Fig. 1(a). In the unit cell, there are two atoms in each Ca and As plane, and four in the Fe plane. Since the orthorhombicity observed in the bulk is extremely small [$(a-b)/(a+b) \sim 0.5\%$] [23], we use the tetragonal unit cell notation. The STM image in Fig. 1(b) shows rows of atoms (stripes) with a spacing of ~8 Å, which is about twice the tetragonal lattice constant a (~4 Å). This is consistent with previous observation at 4.2 K [24]. Surface twin domains are observed as perpendicular stripes by STM (not shown).

Figure 2(a) shows a typical LEED pattern on the surface of $CaFe_2As_2$ obtained at 120 eV. The colored circles show the integer spots [(1,0) and (1,1)], and the fractional spots [(1, 1/2) and (1, 3/2)]. Fractional spots are present in both directions due to the presence of twin domains. We find that the fractional spots are fragile and their existence and sharpness are sensitive to temperature, vacuum, thermal process, and beam energy, similar to doped Ba122 compounds [25]. Thus, extra care has been taken to record the best LEED I-V data in a time period as short as possible, following the fresh cleave at 85 K.

When analyzing the surface structure, we assume that the termination layer cannot be Fe, because of its strong bonding with As. Figures 2(b)–2(g) show six structural models of Ca and As termination. All these models are based on the same (1×2) unit cell, as seen by LEED and STM. Nine (1×2) fractional I-V beams with a total energy range 1224 eV are used to determine the optimal structure. The Pendry R_p factor is used to quantify the goodness of the fit between the calculated and measured I-V curves [26]. The R_p values achieved on the optimized structures for the six different models of the surface of $CaFe_2As_2$ are 0.8 for a full-As dimer [Fig. 2(e)], 0.6 for a full-As rumple [Fig. 2(f)], 0.8 for a half As [Fig. 2(g)], 0.8 for full-Ca dimer [Fig. 2(b)], 0.6 for full-Ca rumple [Fig. 2(c)], and 0.23 for half Ca [Fig. 2(d)]. The half-monolayer-Ca model

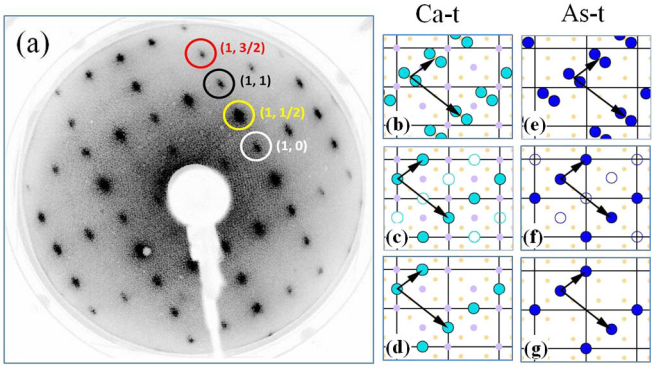

FIG. 2 (color online). (a) A LEED pattern on the surface of $CaFe_2As_2$ (120 eV); (b)–(g): Six possible structural models for the stripe (1×2) phase for Ca (Ca-t) or As (As-t) termination.

TABLE I. Detail stripe (1 × 2) surface structure of Ca122 and 7.5% Co-doped Ca122.

	$Ca(Fe_{1-x}Co_x)_2As_2$ $(x = 0, 0.075)$ (Å)				
Labels	Bulk expt. [7]	Bulk DFT	Surface LEED $x = 0$	Surface LEED $x = 0.075$	Surface DFT
Ca	0.0000	0.000	+0.49 (±0.04)	+0.54 (±0.03)	+0.474
As2	1.5583	1.538	−0.16 (±0.26)	−0.04 (±0.23)	−0.118
Fe1	2.9160	2.851	−0.10 (±0.05)	−0.07 (±0.04)	−0.073
Fe2	2.9160	2.851	−0.01 (±0.10)	+0.08 (±0.13)	−0.043
Fe3	2.9160	2.851	+0.04 (±0.06)	+0.11 (±0.05)	+0.004
As1	4.2737	4.160	−0.11 (±0.10)	−0.04 (±0.06)	−0.072
As3	4.2737	4.160	+0.10 (±0.10)	+0.11 (±0.05)	−0.008
Ca	5.8320	5.698	0.00	0.00	+0.000

is therefore the only acceptable structure, based on its Pendry factor. Table I lists the experimentally determined displacements and our LEED *I-V* structure analysis on $x = 0, 0.075$ compounds.

The preference for the half-monolayer Ca terminated structure is not surprising: it is the most intuitive model and also has the lowest DFT energy [27]. What is surprising is the consequence of the surface reconstruction: Ca atoms at the surface are pulled down (inward relaxation) by ∼0.5 Å as shown in Fig. 3(a). Even more startling is the rippling in the As-Fe_2-As triple layer just below the surface Ca plane: the Fe atoms (Fe1) between the Ca rows move up by ∼0.1 Å compared to the position of this plane for the bulk

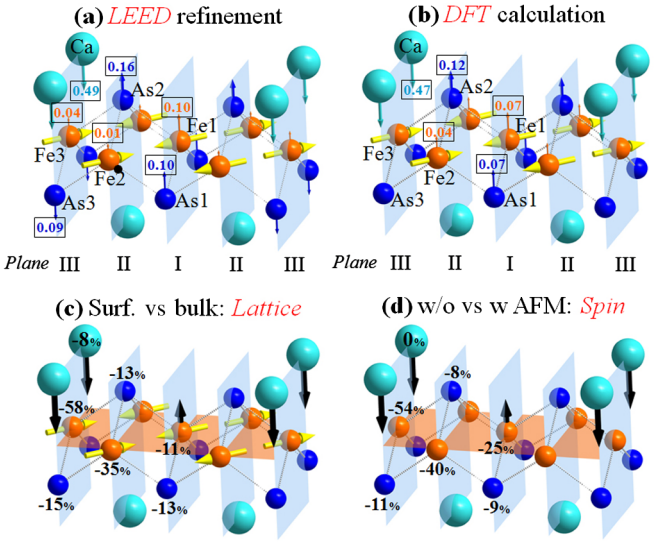

FIG. 3 (color online). (a) Surface structure determined by LEED *I-V* analysis; (b) DFT calculated structure with AFM ordering identical to bulk. In (a),(b), the surface atomic displacements with respect to bulk-projected atomic positions are indicated by arrows accompanied with the values; (c) Bader charge difference between surface and bulk atoms both with AFM ordering. The yellow arrows represent spins while the black arrows indicate the distortion with respect to the bulk; (d) Bader charge difference of surface atoms with (W) and without (W/O) AFM ordering.

structure or the position of Fe3 atoms. The displacements of other surface Fe atoms (Fe2 and Fe3) are less than 0.05 Å, which is comparable to the experimental error bar (see Table I). The R_p value is very sensitive to the vertical motion of Ca and Fe1 atoms, yielding small error bars. The rippling in the Fe plane seems to be accompanied by similar distortion in the As plane (see Table I). The Fe and As atoms are labeled according to their respective planes, with Fe1 and As1 in plane I, Fe2 and As2 in plane II, and Fe3 and As3 in plane III as shown in Figs. 3(a) and 3(b).

To examine the origin of this reconstruction, we performed SDDFT calculations and found that the surface with the bulk AFM ordering—with spins ferromagnetically (FM) coupled along the *b* axis and antiferromagnetically coupled along the *a* and *c* axes [see Fig. 1(a)]—has the lowest energy and reproduces the experiment-determined structure. Here are four important findings. First, in a nonspin polarized calculation, the surface Ca atoms have only 0.38 Å inward relaxation with the bulk orthorhombic structure. Second, when FM ordering is considered, the self-consistent magnetic moment goes to zero, and the structure becomes the collapsed tetragonal phase. Third, among six different AFM orders considered in our calculations, about 0.47 Å surface relaxation is present if and only if the surface has the same AFM ordering as the bulk [Fig. 3(b)]. Within the error bar, this is identical to the experiment-determined inward motion of ∼0.5 Å [Fig. 3(a)]. Finally, theory reproduces the buckling of the center Fe1 atom. These results confirm that the topmost Fe layer in the (1 × 2) orthorhombic $CaFe_2As_2$ surface structure has an AFM ordering similar to the bulk. In other words, the striped (1 × 2) surface structure with a top Ca layer ∼0.5 Å relaxation is the signature of a specific AFM ordering. This signature of AFM ordering can be used in conjunction with STM and STS to determine the coexistence of SC and AFM at the surface.

Since the SDDFT calculations reproduce the observed surface structure with bulk AFM ordering, they can be used to further understand the interplay between spin, charge, and lattice associated with the surface relaxation. The formal valences in Ca122 are Ca^{2+}, Fe^{2+}, and As^{3-}.

TABLE II. Bader charges for orthorhombic surface and bulk with or without including spin ordering.

DFT		Ca1	Fe1	Fe2	Fe3	As1	As2	As3
Orthorhombic AFM	Bulk	+1.43	+0.31	+0.31	+0.31	−1.06	−0.99	−1.05
	Surface	+1.31	+0.28	+0.2	+0.13	−0.92	−0.86	−0.89
Surface-Bulk		−0.12	−0.03	−0.11	−0.18	+0.14	+0.13	+0.16
Orthorhombic nonmagnetic (NM)	Bulk	+1.39	+0.14	+0.14	+0.14	−0.88	−0.79	−0.88
	Surface	+1.31	+0.21	+0.12	+0.06	−0.84	−0.79	−0.79
NM-AFM (bulk)		−0.04	−0.17	−0.17	−0.17	+0.18	+0.2	+0.17
NM-AFM (surface)		0.00	−0.07	−0.08	−0.07	+0.08	+0.07	+0.10

Figure 3(c) and Table II show the calculated change in the charge on the surface atoms compared to the equivalent atoms in the bulk. Overall, the surface becomes more neutral (i.e., less ionic) than the bulk. For example, the surface Ca atoms, which are pulled down by ∼0.5 Å, become 8% less positively charged (+1.43e in the bulk to +1.31e at the surface), and the Fe3 atom becomes ∼58% less positive (+0.31e in the bulk to +0.13e at the surface). On average, the charge on the Fe layer (the third layer) is reduced by ∼34% compared to its bulk counterpart. The charge rearrangement is also present in the second and forth As layers, all becoming 13%–15% less negative. This is clearly a signature of the interplay between charge distribution and surface reconstruction. We also calculated the effect of spin ordering on the charge distribution by constraining the magnetic moment to be zero, i.e., nonmagnetic (NM), and keeping the orthorhombic structure. Figure 3(d) and Table II shows that there is significant charge redistribution on the orthorhombic NM surface compared to the orthorhombic AFM case. The negatively charged As atoms become less negative and the positively charged Fe atoms become less positive. The removal of spin ordering reduces the electronic charge transfer from Fe atoms to As atoms. This indicates that the charge redistribution is coupled with spin arrangement.

It was previously observed that the surface reconstruction could suppress superconductivity for the p-wave superconductor Sr_2RuO_4, making STS unable to probe superconducting gap [28,29]. This is not the case here since we see the signature of a SC gap below T_c for $Ca(Fe_{0.925}Co_{0.075})_2As_2$. Figure 4(a) shows the averaged STS taken from the clean (1 × 2) surface [Figs. 4(b)–4(c) of $Ca(Fe_{0.925}Co_{0.075})_2As_2$ at 20, 16, and 7.4 K, respectively. There is no gap feature down to 16 K, indicating that the transition temperature at the surface is lower than that in the bulk. However, coherence peaks are seen at 7.4 K, due to the SC gap $\Delta \sim 7.5$ meV. The naive interpretation is that superconductivity coexists with antiferromagnetic ordering at the (1 × 2) surface. However, our structural determination is performed at 80 K, and could be different at temperatures below T_c, and there is a large zero-bias conductance, nearly half of that at the coherence peak.

Since the (1 × 2) striped structure is the signature of AFM ordering, it is essential to prove that the surface structure does not change as the sample becomes superconducting. Neutron scattering measurements do not show a structural or magnetic moment change when crossing T_c of Ca122 [30]. However, such measurements have no spatial resolution. At the surface, our STM topographies taken with the same tip and the same tunneling junction show no change in atomic corrugation and surface adatom (bright protrusion) height above and below T_c [Figs. 4(b)–4(d)]. As demonstrated in Fig. 3, any change in lattice structure and/or magnetic ordering would result in large charge redistribution. The unchanged atomic corrugation in STM images across T_c confirms the same lattice structure and spin ordering below T_c.

Zero-bias conductance was previously observed on the (1 × 2) surface of Ca122 with superconductivity induced by partial substitution of Ca using La [31]. If the tunneling spectra shown in Fig. 4(a) were from a tunnel junction measurement, the interpretation would be obvious: superconducting region (with gap) coexisting with nonsuperconducting region (with finite zero-bias conductance). However, STM and STS measurements are spatially

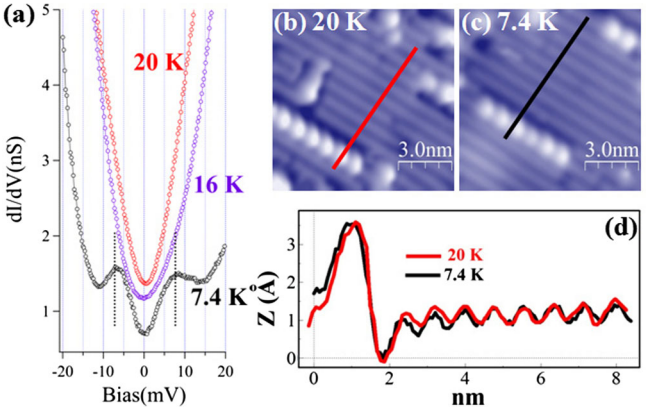

FIG. 4 (color online). (a) Averaged STS taken from the clean stripe (1 × 2) surface of $Ca(Fe_{0.925}Co_{0.075})_2As_2$ at the indicated temperatures; (b) and (c) STM topographic images taken at 20 and 7.4 K, respectively ($V_{bias} = 1.0$ V, $I_t = 200$ pA). The profiles along indicated lines in (b) and (c) are shown in (d).

resolved (in plane) on a scale much smaller than the coherence length or the domain size. If the measurement is sampling an inhomogeneous material, it has to be in the direction perpendicular to the surface. For Ca122, STS may have contributions from the reconstructed surface that tends to be a normal metal and the bulk which is superconducting. The latter penetrates into the surface via the proximity effect, thus revealing the features of a superconducting gap (e.g., coherence peaks in STS). This is consistent with our observation that the gap feature in STS disappears at 16 K [Fig. 4(a)], lower than the bulk T_c, very similar to a STM and STS observation of the proximity effect on heterogeneous superconducting thin films on metallic substrates [32]. This scenario can explain the observed variation of the zero-bias conductance for different reconstructed phases of the $A122$ system [33].

In summary, we have carried out LEED I-V analysis to identify the stripe-ordered phase observed at the surface of $Ca(Fe_{1-x}Co_x)_2As_2$ ($x = 0$ and 0.075). The surface consists of half-Ca layer with a (1×2) structure. These surface Ca atoms move inward $\sim$0.5 Å and the surface As-Fe_2-As layer is buckled. DFT calculations show that the (1×2) phase is stabilized by the bulk antiferromagnetic ordering through the spin-charge-lattice coupling, providing a signature of AMF ordering at the surface. Furthermore, STS measurements show the presence of a superconducting gap on the ordered (1×2) surface, while the spectra always have a finite zero-bias conductance. These observations result from a combination of the reconstructed surface, which tends to be both AFM ordered and superconducting due to the proximity to the superconducting bulk. The surface-stabilized coexistence of superconductivity and AFM ordering raises the prospect of growing artificial structured materials with this property.

Research at LSU is partially supported by NSF DMR-1002622 (G. L., R. J., E. W. P.) and DMR-1005562 (J. D.). Research at RPI is supported by the New York State under NYSTAR Contract No. C080117. Research at the CNMS (Q. L., M. P.) user facility at ORNL is supported by DOE. We would like to thank Jisun Kim for useful discussions.

[1] S. Nandi *et al.*, Phys. Rev. Lett. **104**, 057006 (2010).
[2] J. Teng, C. Chen, Y. Xiong, J. Zhang, R. Jin, and E. W. Plummer, Proc. Natl. Acad. Sci. U.S.A. **110**, 898 (2013).
[3] J. E. Hoffman, Rep. Prog. Phys. **74**, 124513 (2011).
[4] Y. Kamihara, T. Watanabe, M. Hirano, and H. Hosono, J. Am. Chem. Soc. **130**, 3296 (2008).
[5] D. C. Johnston, Adv. Phys. **59**, 803 (2010).
[6] G. Li, X. He, J. Zhang, R. Jin, A. S. Sefat, M. A. McGuire, D. G. Mandrus, B. C. Sales, and E. W. Plummer, Phys. Rev. B **86**, 060512 (2012).
[7] L. Harnagea *et al.*, Phys. Rev. B **83**, 094523 (2011).
[8] J. J. Wu, J.-F. Lin, X. C. Wang, Q. Q. Liu, J. L. Zhu, Y. M. Xiao, P. Chow, and C. Jin, Proc. Natl. Acad. Sci. U.S.A. **110**, 17263 (2013).
[9] Y. Kamihara *et al.*, New J. Phys. **12**, 033005 (2010).
[10] J. Zhao *et al.*, Nat. Mater. **7**, 953 (2008).
[11] L. Ma, G. F. Ji, J. Dai, X. R. Lu, M. J. Eom, J. S. Kim, B. Normand, and W. Yu, Phys. Rev. Lett. **109**, 197002 (2012).
[12] A. Li, J. Ma, A. Sefat, M. McGuire, B. Sales, D. Mandrus, R. Jin, C. Zhang, P. Dai, and S. Pan, Bull. Am. Phys. Soc. **B23**, 133 (2011).
[13] S. Pan, A. Li, J. Ma, J. O'Neal, A. Sefat, M. McGuire, B. Sales, D. Mandrus, R. Jin, and E. W. Plummer, Bull. Am. Phys. Soc. **T39**, 467 (2010).
[14] C. Dhital, Z. Yamani, W. Tian, J. Zeretsky, A. S. Sefat, Z. Wang, R. J. Birgeneau, and S. D. Wilson, Phys. Rev. Lett. **108**, 087001 (2012).
[15] P. Cai, X. Zhou, W. Ruan, A. Wang, X. Chen, D.-H. Lee, and Y. Wang, Nat. Commun. **4**, 1596 (2013).
[16] F. Ronning, T. Klimczuk, E. D. Bauer, H. Volz, and J. D. Thompson, J. Phys. Condens. Matter **20**, 322201 (2008).
[17] S. H. Pan, E. W. Hudson, and J. C. Davis, Rev. Sci. Instrum. **70**, 1459 (1999).
[18] G. Kresse and J. Furthmüller, Comput. Mater. Sci. **6**, 15 (1996).
[19] G. Kresse and J. Furthmüller, Phys. Rev. B **54**, 11169 (1996).
[20] J. P. Perdew, K. Burke, and M. Ernzerhof, Phys. Rev. Lett. **77**, 3865 (1996).
[21] P. E. Blöchl, Phys. Rev. B **50**, 17953 (1994).
[22] H. J. Monkhorst and J. D. Pack, Phys. Rev. B **13**, 5188 (1976).
[23] A. Goldman, D. Argyriou, B. Ouladdiaf, T. Chatterji, A. Kreyssig, S. Nandi, N. Ni, S. Bud'ko, P. Canfield, and R. McQueeney, Phys. Rev. B **78**, 100506 (2008).
[24] T.-M. Chuang, M. P. Allan, J. Lee, Y. Xie, N. Ni, S. L. Bud'ko, G. S. Boebinger, P. C. Canfield, and J. C. Davis, Science **327**, 181 (2010).
[25] E. van Heumen *et al.*, Phys. Rev. Lett. **106**, 027002 (2011).
[26] J. B. Pendry, J. Phys. C **13**, 937 (1980).
[27] M. Gao, F. Ma, Z.-Y. Lu, and T. Xiang, Phys. Rev. B **81**, 193409 (2010).
[28] R. Matzdorf, Z. Fang, Ismail. Jiandi Zhang, T. Kimura, Y. Tokura, K. Terakura, and E. W. Plummer, Science **289**, 746 (2000).
[29] C. Lupien, S. K. Dutta, B. I. Barker, Y. Maeno, and J. C. Davis, arXiv:cond-mat/0503317v1.
[30] K. Prokeš, S. Mat'aš, L. Harnagea, S. Singh, S. Wurmehl, D. N. Argyriou, and B. Büchner, Phys. Rev. B **83**, 104414 (2011).
[31] H. Yao-Bo *et al.*, Chin. Phys. Lett. **30**, 017402 (2013).
[32] J. Kim, V. Chua, G. A. Flete, H. Nam, A. H. MacDonald, and C. K. Shih, Nat. Phys. **8**, 464 (2012).
[33] J. Kim *et al.* (to be published).